(1)

National Défense
Defence nationale

A DOPPLER BIN BLANKING CFAR PROCESSOR FOR AIRBORNE RADARS

by

G. Vrckovnik and D. Faubert

DEFENCE RESEARCH ESTABLISHMENT OTTAWA
REPORT NO. 1073

Canada

April 1991
Ottawa

National Défense
Defence nationale

A DOPPLER BIN BLANKING CFAR PROCESSOR FOR AIRBORNE RADARS

by

G. Vrckovnik and D. Faubert
Airborne Radar Section
Radar Division

DEFENCE RESEARCH ESTABLISHMENT OTTAWA
REPORT NO. 1073

PCN
021LA

April 1991
Ottawa

ABSTRACT

In this report a novel scheme for adaptively "blanking-out" the radar resolution cells which contain high clutter interference is developed and investigated. For the particular set of radar parameters that are used, a 60 dB clutter peak appears across all of the range gates, and many of the Doppler bins. If not dealt with, this huge peak severely degrades the performance of the CFAR processor, and reduces the sensitivity of the system to targets which reside outside of the clutter region. Our technique consists of adaptively excluding from the decision process, the range-Doppler cells located within this clutter peak region. As a result, the performance in the noise dominated interference region is greatly enhanced. Blanking out the clutter peak also reduces the variation which occurs in the values of the CFAR threshold multiplier over various geometric conditions in which the radar may be operated. It is shown that a single value of the CFAR constant can maintain the false alarm rate for large differences in the operating environment of the radar, if Doppler bin blanking is employed. Consequently, a much simpler CFAR processor can be implemented.

RÉSUMÉ

Dans ce rapport, une nouvelle méthode pour éliminer les cellules de résolution radar contenant un haut niveau d'interférence est développée et étudiée. Pour l'ensemble des paramètres du radar utilisés, un pic de fouillis de 60 dB apparaît dans toutes les cellules de portées et dans plusieurs cellules Doppler. Sans traitement approprié, cet énorme pic de fouillis dégrade sérieusement la performance du processeur CFAR et réduit la sensibilité du système aux cibles à l'extérieur de la zone de haute interférence. De façon adaptive, notre technique consiste à exclure du processus de décision la région d'interférence à l'intérieur de laquelle il est de toute façon fort improbable de détecter des cibles. La performance du système dans la région dominée par le bruit thermique s'en trouve grandement améliorée. Aussi, l'élimination du pic de fouillis réduit la variation du multiplicateur CFAR quand la géometrie dans laquelle le radar opère change. Avec notre technique, une seule valeur de la constante CFAR suffit même lorsque l'environnement dans lequel le radar opère varie beaucoup. Par conséquent, un processeur CFAR beaucoup plus simple peut être implanté.

EXECUTIVE SUMMARY

Constant false alarm rate (CFAR) processors are used to prevent automatic detection radar systems from becoming overloaded with false targets, in the presence of time-varying or unknown interference environments. They maintain the number of false alarms at a level consistent with the design goals. Unfortunately, large clutter returns can cause severe degradation in the performance of these processors. The degradation manifests itself as a reduction in the ability to detect targets of a given signal-to-noise ratio, while maintaining the overall system false alarm rate. As well, the constant multiplying factor used in CFAR processors tends to vary as the range-Doppler resolution cell map changes.

In this report a novel adaptive algorithm to exclude the range-Doppler cells which contain clutter is developed. This algorithm, when used in conjunction with a CFAR processor, greatly enhances the system's sensitivity to targets which reside in the clutter-free region of the range-Doppler map. It is also shown that the CFAR multiplier is relatively invariant to changes in the geometric conditions of the radar, when the adaptive Doppler bin blanking scheme is used. This blanking scheme could lead to a simple CFAR processor which would be effective in any possible clutter environment.

TABLE OF CONTENTS

LIST OF FIGURES

LIST OF TABLES

1.0 INTRODUCTION

In modern radar systems, automatic detection schemes compare some function of the envelope detector output, in a range-Doppler resolution cell, with a threshold number. A target is declared to be present if the threshold is exceeded. The threshold value is selected to provide a false alarm rate consistent with the operational goals, without overloading the radar system signal and data processors. Increasing the detection threshold unnecessarily, results in a desensitization of the radar system to target returns.

The threshold value is a product of the ambient interference power and a proportionality constant controlling the false alarm rate. Unfortunately, the interference power in real operating environments is not constant because it consists of thermal noise plus the return echoes from many point, area or extended targets, known as clutter. When the automatic detection scheme assumes a constant interference power, the false alarm probability is extremely sensitive to small variations in that interference power [1]. Since all radar systems operate in time-varying, and unknown interference environments, automatic detection schemes which employ fixed thresholds are not practical .

The problems of automatic target detection in interference environments which are unknown, or time varying, can be reduced with the use of constant false alarm rate (CFAR) processors. A CFAR processor maintains a constant false alarm probability, while maximizing the detection probability, by estimating the interference power in the resolution cell under test. If the power in this resolution cell exceeds some fixed multiple of the estimated interference power, then a target is declared to be present.

In a previous report [2], three different CFAR techniques (cell-averaging, greatest-of, and smallest-of [3]) were applied to simulated airborne pulse-Doppler radar data. Interference environments of thermal noise, and thermal noise plus clutter were considered. The interference power distribution in the cell under test was assumed to be known, except for the mean power μ_i. The distribution family used was exponential, which corresponds to an interference environment having a Rayleigh-envelope clutter distribution. The same assumptions about the interference statistics will be made for the work in this report.

It was found in [2] that the CFAR processors worked very well in the thermal noise environment (CFAR losses < 0.6 dB), but a severe peak in the clutter environment caused serious degradations in their performance. In this report, a modification is suggested which greatly improves the processors' performance in clutter. By adaptively "blanking out" the range-Doppler resolution cells which contain clutter, the CFAR processor performance becomes equivalent to the excellent performance achieved in the thermal noise environment. Also, by removing the cells containing clutter, one threshold proportionality constant can be used in any radar geometry (look angle, altitude etc.) to yield the desired false alarm probability, as opposed to having to compute a new multiplier each time the geometric conditions change.

2.0 CFAR DESCRIPTION

The CFAR processor estimates the mean power, $\hat{\mu}_i$, of the interference in the i^{th} cell under test. The squared modulus of the signal in the cell under test is then compared to a threshold, T_i, where

$$T_i = C\hat{\mu}_i , \tag{1}$$

and C is a constant controlling the probability of false alarm. C is known by several names: the CFAR constant, the threshold multiplier, or the threshold constant. If the actual power in the cell under test exceeds the threshold in (1), then a target detection is declared.

The value of C which produces a desired false alarm probability of P_{FAdes}, with exact mean estimation is,

$$C_0 = F_u^{-1}(1-P_{FAdes}) , \tag{2}$$

where $F_u(x)$ is the unit mean distribution of the exponential distribution family, given by [4]

$$F_u(x) = 1 - e^{-x} . \tag{3}$$

Thus the optimal values of C for the desired false alarm probabilities of $P_{FAdes} = 10^{-3}$, and 10^{-6}, are $C_0 = 8.39$ dB and 11.40 dB, respectively. A technique for determining the threshold multiplier C, which yields the desired false alarm rate P_{FAdes} for any CFAR processor, was derived by Weber and Haykin [4]. As this technique was described in detail in [2], only a brief summary will be given here.

The CFAR algorithm being tested estimates the mean power in each cell, $\hat{\mu}_i$, of each range-Doppler map in the ensemble of snapshots. An estimation error for each cell is computed as the ratio $\hat{\mu}_i/\mu_i$, in which μ_i is the mean power of the cell calculated over the ensemble of snapshots. The natural logarithm of the estimation error is computed for all of the cells in the ensemble of snapshots, and a global log-estimation-error histogram, $f_{ln(\hat{\mu}/\mu)}(x)$, is formed.

The system false alarm probability can be determined using this log-error histogram, the CFAR constant C, and knowledge of the distribution family. This results from the fact that P_{FA} is only dependent upon the ratio of the threshold and the mean power, not upon their actual values. P_{FA}, as a function of $ln\ C$, is found by correlating the global log-error histogram with the function $1 - F_u(e^x)$. The log-error histogram need only be taken once, for $C = 1$, since the log-error histogram shifts to the right or left, depending upon the value of C. Determining the value of C, which yields the desired probability of false alarm, P_{FAdes}, is a trial and error process involving iterative solutions of the correlation. A search algorithm, based upon the Van Wijngaarden-Dekker-Brent method [5], was implemented to determine the value of C which resulted in a false alarm probability within one one-thousandth of the desired probability of false alarm.

The different CFAR techniques all have different biases and variances, hence comparing only C values between the techniques is meaningless. By forming histograms of the estimated powers in each cell $\hat{\mu}_i$, a cumulative distribution function of the estimated powers can be found, $F_{est}(x)$. Once the value of C has been computed, the cumulative distribution function of the threshold can be found, using (1), from [6],

$$F_T(x) = F_{est}\left(\frac{x}{C}\right) \tag{4}$$

Comparison of the threshold distribution functions, $F_T(x)$, can be used to rate the performance of different CFAR techniques. If $F_T(x)$, for one CFAR method, is strictly to the left (or above) of the $F_T(x)$, from another CFAR method, then the first algorithm is better because it will produce a smaller false alarm probability for any value of the return echo power. The horizontal distance between the threshold distributions is the difference in CFAR loss between the methods, for a steady target at a detection probability of $P_D = F_T$. The absolute CFAR loss can be found by comparing $F_T(x)$ to the distribution of the thresholds for an ideal receiver, in which $T_i = C_0\mu_i$.

3.0 AIRBORNE RADAR DATA GENERATION

The DREO airborne radar simulator (ABRSIM) [7-11] was used to generate the interference in the Doppler bin outputs, of each range gate, of an airborne pulse-Doppler radar. The relevant radar parameters in the simulation include a pulse width of 3.33 μs and a pulse repetition frequency of 50 kHz. As a result, a total of five contiguous range gates (whose centres are spaced 500 m apart), and 128 Doppler frequency bins, make up the range-Doppler map of any particular snapshot.

The simulator was run in its covariance matrix computation mode with the radar flying at three different altitudes: 100 m, 1 km, and 10 km; and the antenna pointing in two different directions : forward looking, and side looking. The aircraft's velocity was 330 m/s in each case. In the covariance matrix computation mode, the simulator computes the cross-correlation matrix of the range gate samples. In effect, this simulator mode computes an ensemble average of an infinite number of snapshots. The effects of the antenna backlobes and sidelobes are included in the result. The antenna backlobes were set to a level of -30 dB with respect to the main lobe of the antenna pattern.

Figures 1 through 6 illustrate the resulting covariance mode range-Doppler interference powe. maps, generated by the simulator, for the 6 different altitude-look angle combinations mentioned above. From these figures two distinct regions can be discerned. In all of the plots, there is a very large peak, extending across all 5 range gates, which is surrounded on both sides by a relatively flat region. This flat region represents the interference power which is dominated by thermal noise. The large peak contains both surface clutter and thermal noise. In effect, the system's performance is clutter limited in the peak region, while noise limited elsewhere.

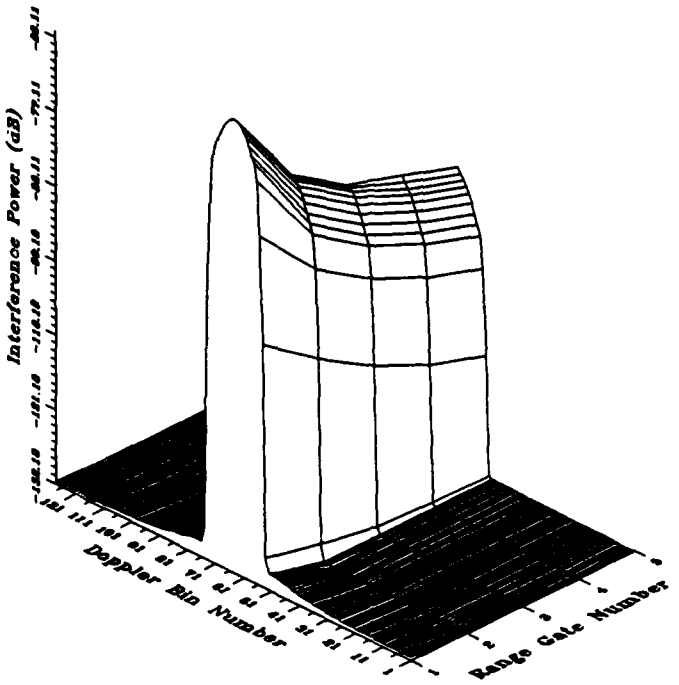

Figure 1 : Sidelook, Altitude = 100 m

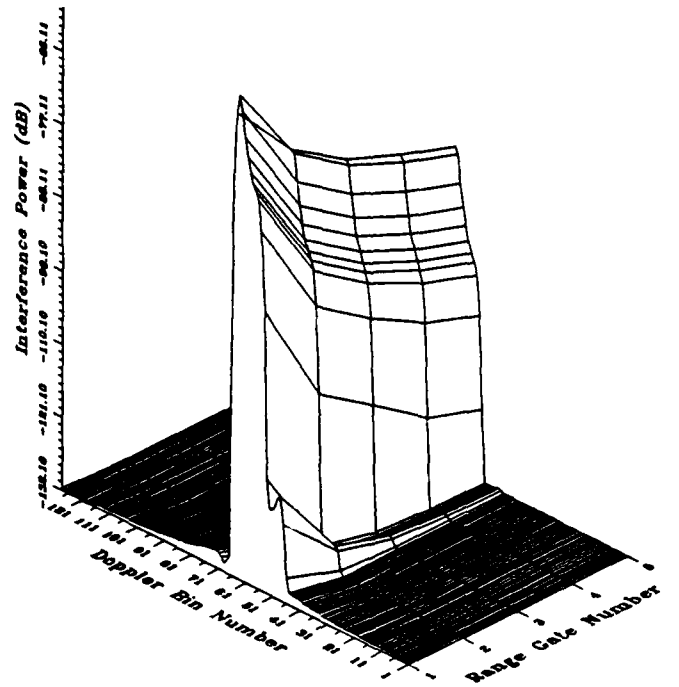

Figure 2 : Forward Look, Altitude = 100 m

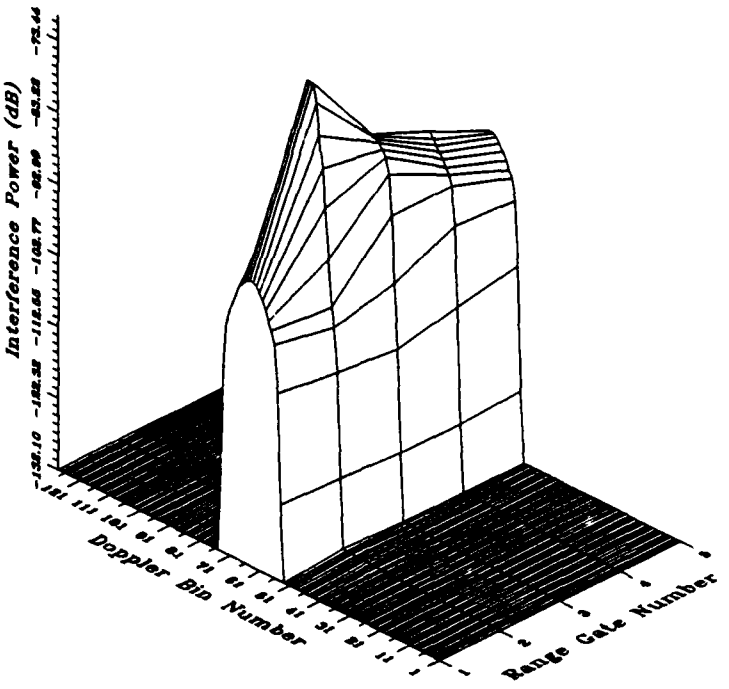

Figure 3 : Sidelook, Altitude = 1 km

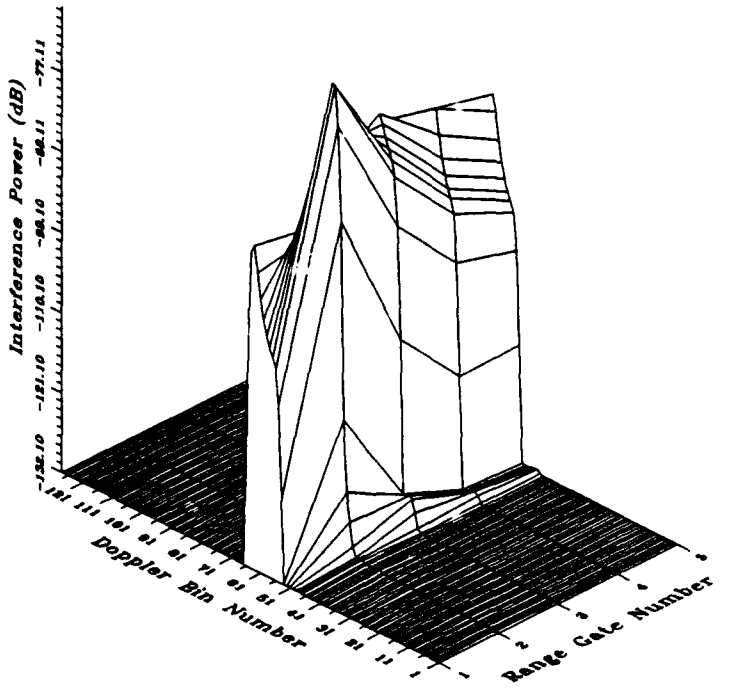

Figure 4 : Forward Look, Altitude = 1 km

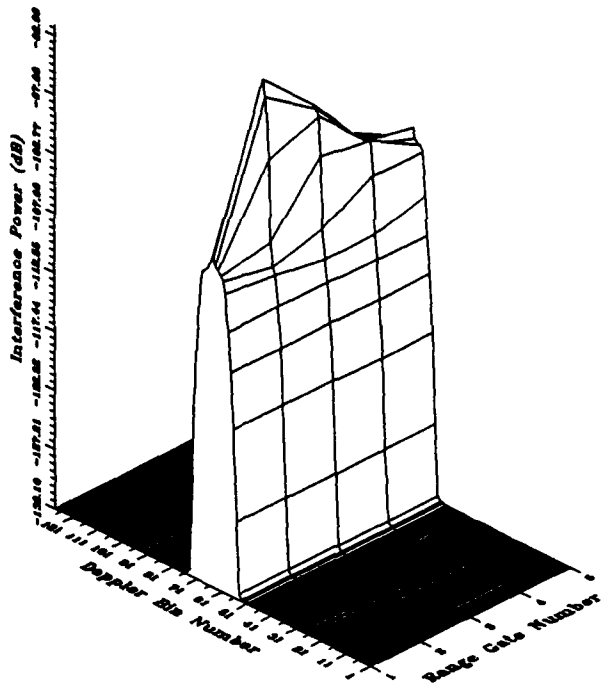

Figure 5 : Sidelook, Altitude = 10 km

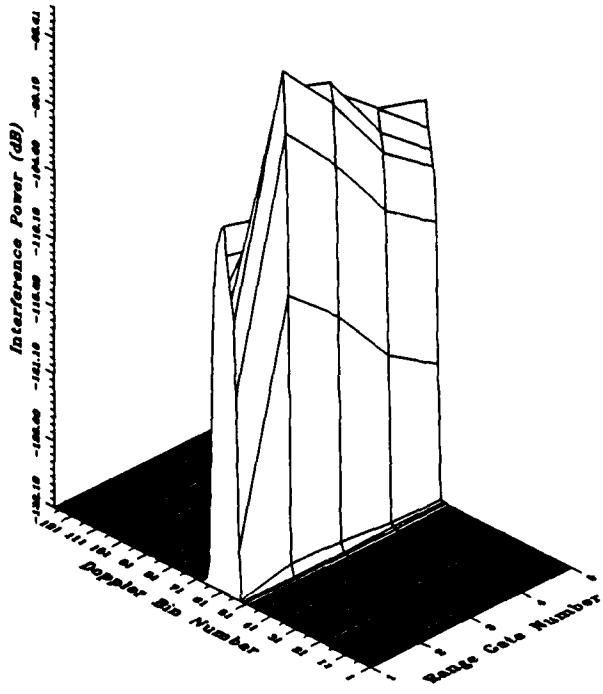

Figure 6 : Forward Look, Altitude = 10 km

The clutter dominated region covers the Doppler velocities of $\pm v_{ac}$, where v_{ac} is the velocity of the aircraft, plus an additional spill-over velocity caused by the window used in the digital signal processing (Blackman-Harris). One can also see the effect of the altitude return in range gate 2, at altitudes of 1 km (Figures 3 and 4) and 10 km (Figures 5 and 6). The reader is referred to the references on ABRSIM for further details and information regarding the simulator's output.

It is assumed that the interference return to any cell in any individual burst is a random variable, having an exponential distribution, independent of the returns to other cells. This is simulated by generating a sequence of unit mean, exponentially distributed random variables, and assigning one to each cell in the range-Doppler map. After scaling these random numbers by the cell mean value, one snapshot from the ensemble of possible returns is generated. The maps produced by the simulator, in the covariance matrix mode, represent the cell mean powers for the range-Doppler maps. Using this technique, it is possible to generate many snapshots of range-Doppler maps, for the various look angle, altitude combinations. This large number of snapshots ensures statistical accuracy in the CFAR simulation results which follow.

4.0 SIMULATION RESULTS

In this section, we compare the cell-averaging CFAR processor with a modified, "Doppler-Blanked" version of it. Consequently, a review of the cell-averaging CFAR processor and its simulation results is given below, followed by the results of the "Doppler Blanking" cell-averaging CFAR processor.

4.1 Cell-Averaging (CA-) CFAR

A cell-averaging CFAR processor estimates the interference power, in the cell under test, by using the average value of the surrounding reference cells. That is,

$$\hat{\mu}_i = \frac{1}{N}\sum_{j=1}^{N} X_j \qquad (5)$$

where $\hat{\mu}_i$ is the estimated power of cell i, X_j is the power in reference cell j, and N is the size of the reference cell set. Because targets are not generally centred in a range gate or a Doppler bin, the range-Doppler cells which immediately surround the test cell are not included in the reference cell set. A further discussion about the reference cell set may be found in [2]. A block diagram of a one-dimensional CA-CFAR processor is given in Figure 7.

An inherent assumption of the CA-CFAR processor is that the interference statistics of each reference cell are identical to the statistics of the test cell. Consequently, the performance of the CA-CFAR processor deteriorates when the interference is nonhomogeneous over the reference cell window. The two most common forms of nonhomogeneity are edge effects and discrete scatterers [3].

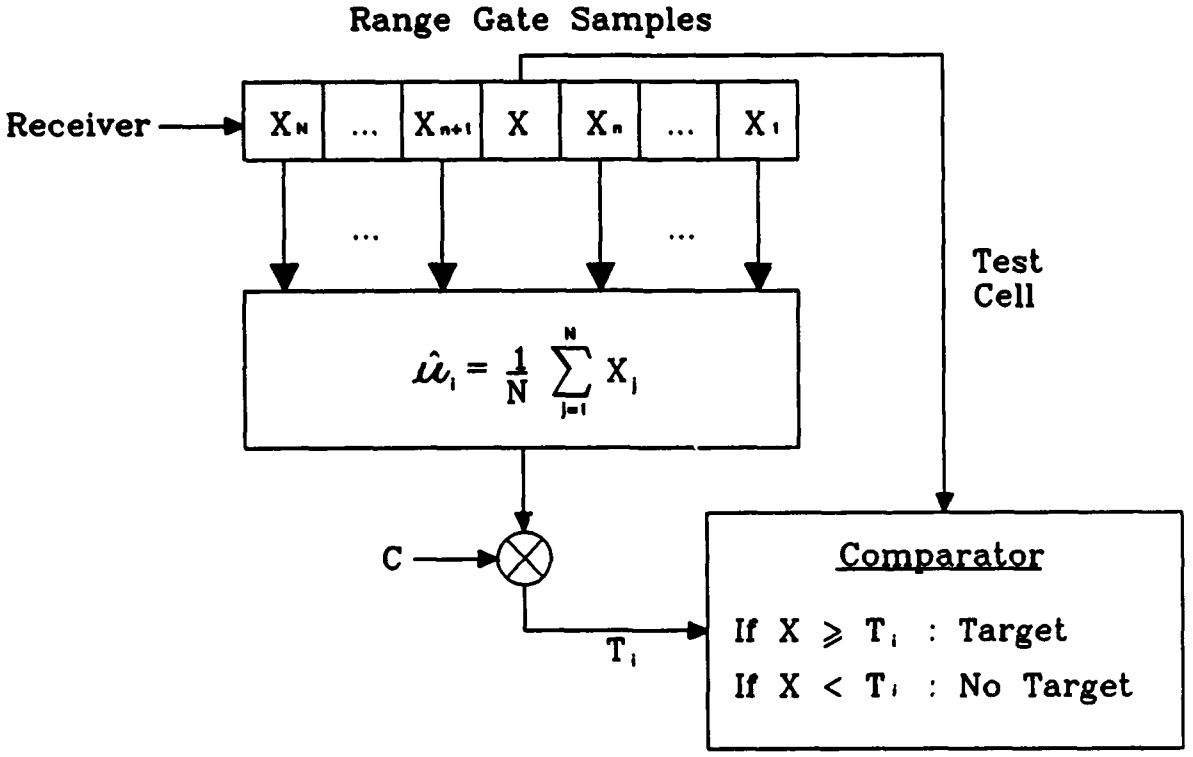

Figure 7 : Cell Averaging CFAR Processor

Edge effects arise when the mean cell powers in the reference window undergo a step change along some boundary. This usually occurs when two or more different clutter environments (ie. land and sea boundary) lie within the reference window.

Two different cases exist for edge effects [12]:

a) If the test cell lies in a region of weak interference, while some of the reference cells are immersed in the clutter edge, then the threshold will be unnecessarily raised, thereby reducing the probability of detection. This can be the case, even though the cell under test has a high signal-to-noise ratio. The clutter regions are expanded by approximately half the length of the reference window, causing a masking effect to occur within the clutter area, and slightly outside of it. The adaptive blanking scheme which we propose can resolve these problems because the clutter region is excluded from the test cell's reference set.

b) If the cell under test is immersed in the clutter edge, but some of the reference cells are in the clear region, then the probability of false alarm increases dramatically as the edge step size increases. This is a serious problem in the design of search radars [13]. Once again, our adaptive blanking scheme solves this problem because detections are not attempted in the cells which reside in the clutter edge.

The presence of a large discrete scatterer, in one or more reference window cells, can cause changes in the clutter distribution itself. This generally occurs when one or more interfering targets lie within the reference window. The resulting increase in the threshold level degrades the detection of the target in the cell under test. The use of an ordered statistic processor, in conjunction with our adaptive blanking scheme, should reduce the effects of a large discrete scatterer [16].

The CA-CFAR processor was tested on each of the six radar geometry conditions. A 4 x 4 (range dimension, Doppler dimension) reference cell set was used, and 350 snapshots were generated to ensure statistical accuracy. A desired false alarm probability of 10^{-3} was selected after considering the memory limitations and speed of the computer which ran the simulation [2]. Results for different reference windows, and different desired false alarm rates, were reported in [2], for a side-looking radar at an altitude of 100 m.

Table 1 presents the threshold multipliers (C), that were computed for each of the six cases. Also listed, is the actual false alarm rate that was obtained for the data which was generated. As expected, this rate is close to the desired rate of 10^{-3}. It is evident from Table 1 that the radar geometry has a significant impact upon the value of the threshold multiplier. This is due to the fact that the magnitude of the clutter peak varies as the radar antenna's altitude and look angle change. Unfortunately, the large variation (6.04 dB) in the threshold multiplier implies that in order to maintain a constant false alarm probability, the threshold multiplier must be recomputed whenever the radar geometry changes. This may or may not be practical, depending upon the platform which carries the radar. Perhaps a look-up table could be used to store multiplier values for various radar geometries instead of recomputing these numbers whenever conditions change.

RADAR GEOMETRY	C (dB)	ACTUAL P_{FA}
Sidelook, Altitude = 100 m	14.258	1.116×10^{-3}
Sidelook, Altitude = 1 km	13.730	9.7767×10^{-4}
Sidelook, Altitude = 10 km	10.890	1.1116×10^{-3}
Forward, Altitude = 100 m	16.928	9.5535×10^{-4}
Forward, Altitude = 1 km	16.603	9.1964×10^{-4}
Forward, Altitude = 10 km	12.807	9.1964×10^{-4}

TABLE 1 : CA-CFAR (4x4) Threshold Multipliers

The threshold distribution functions for each of the six cases, and the corresponding optimal distribution functions, are plotted in Figures 8 to 13. The actual threshold values for the first range gate, averaged over the ensemble of snapshots, are illustrated in Figures 14 to 19, for each of the six cases. The CFAR losses of the various cases are listed in Table 2 for detection probabilities of 0.5 and 0.9. These loss values were obtained by comparing the optimal and actual threshold distribution functions at $F_T(x) = 0.5$ and 0.9, in Figures 8 to 13.

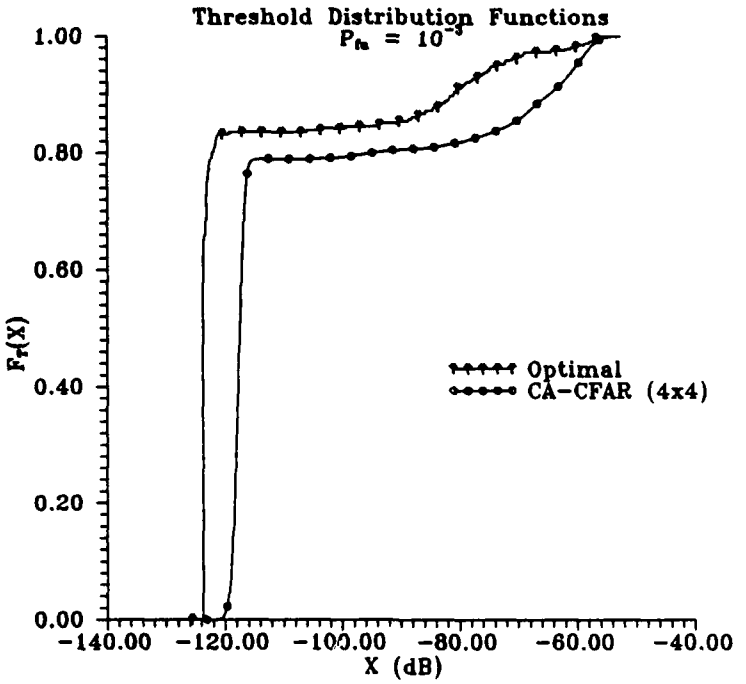

Figure 8: Threshold CDFs - Sidelook, Altitude = 100 m

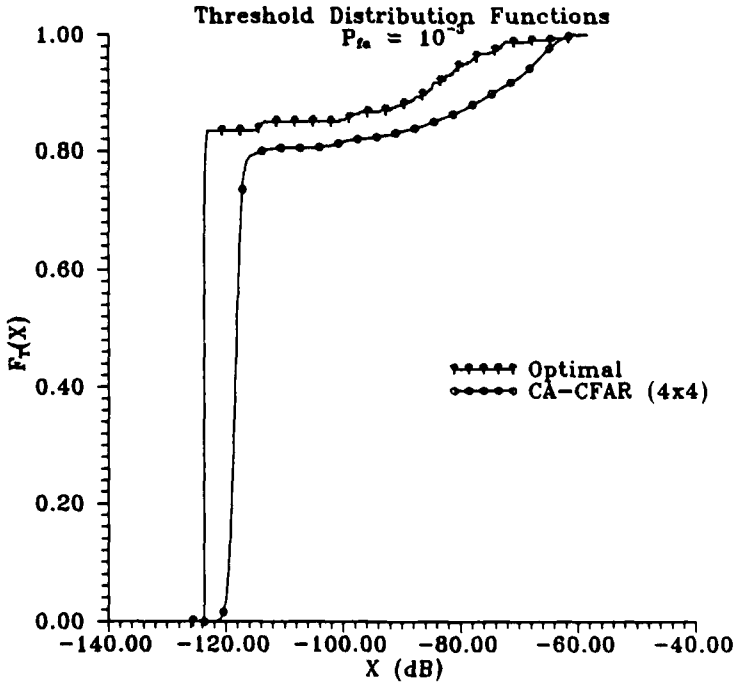

Figure 9: Threshold CDFs - Sidelook, Altitude = 1 km

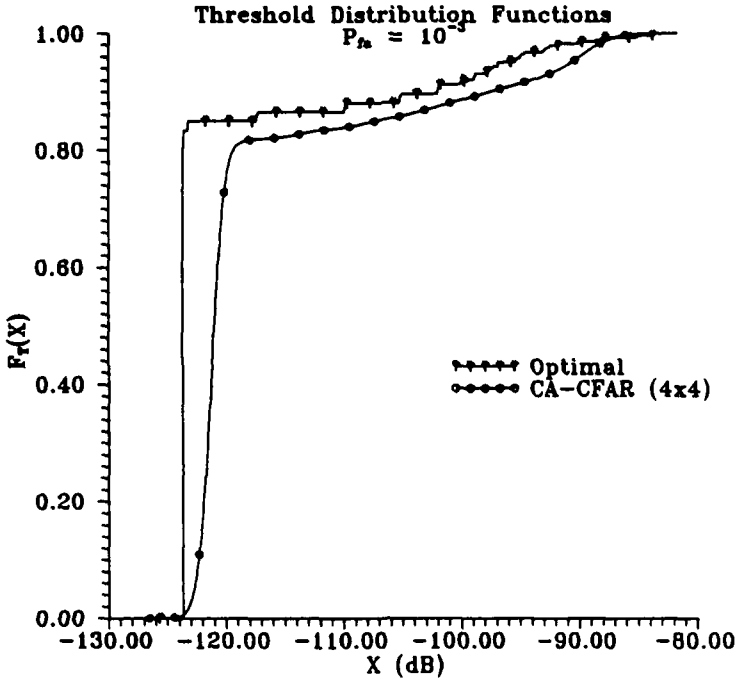

Figure 10: Threshold CDFs - Sidelook, Altitude = 10 km

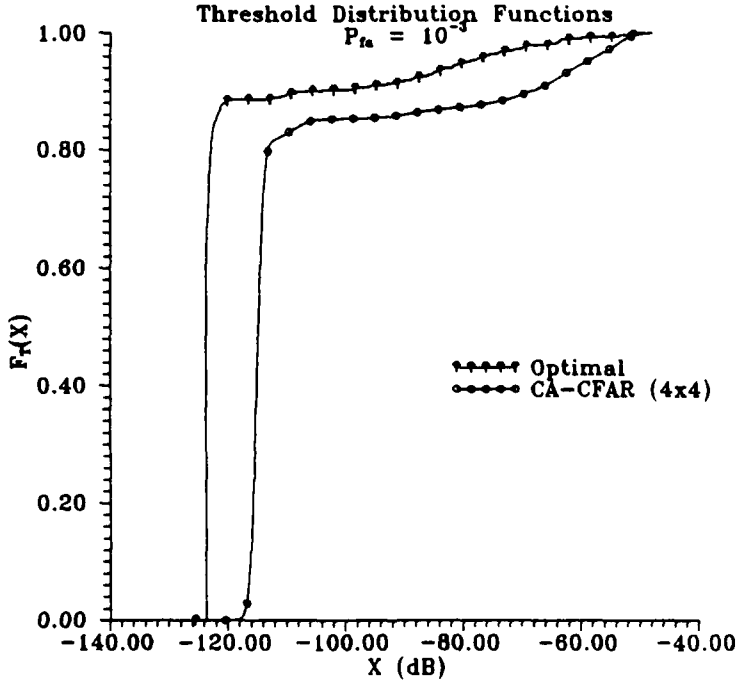

Figure 11: Threshold CDFs - Forward, Altitude = 100 m

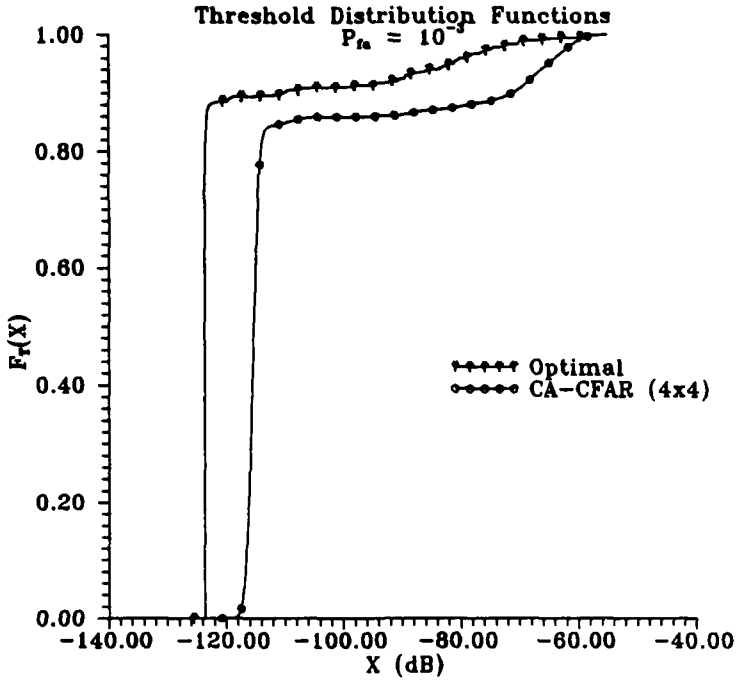

Figure 12: Threshold CDFs - Forward, Altitude = 1 km

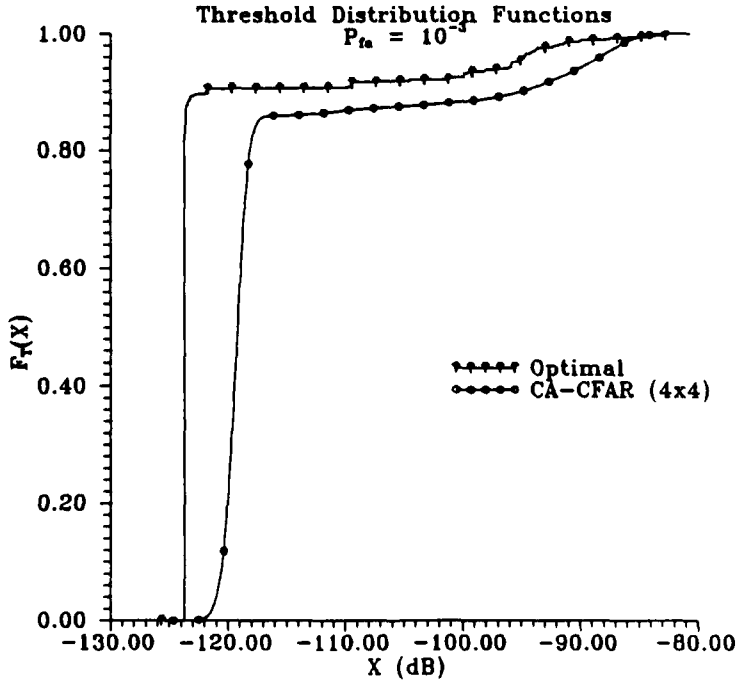

Figure 13: Threshold CDFs - Forward, Altitude = 10 km

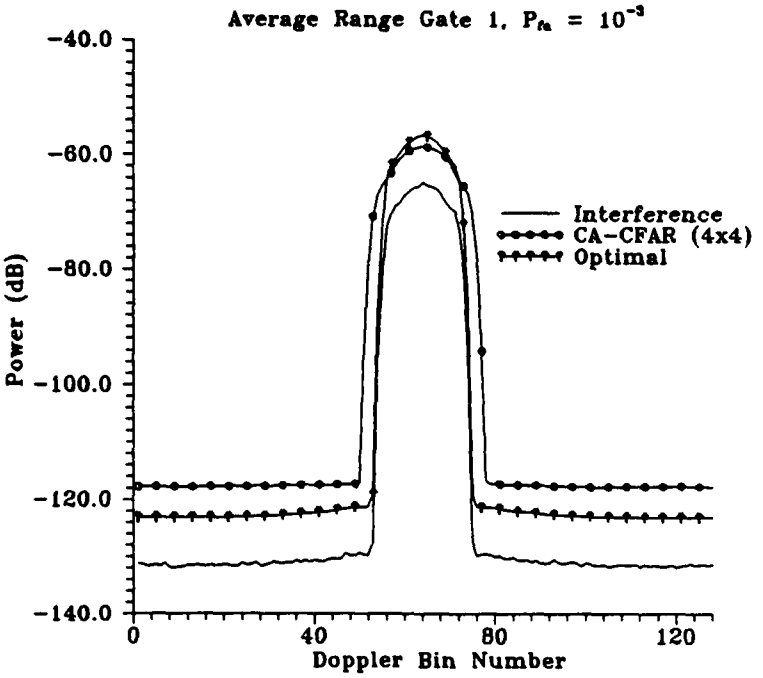

Figure 14 : Threshold Values, RG1, Sidelook, 100 m

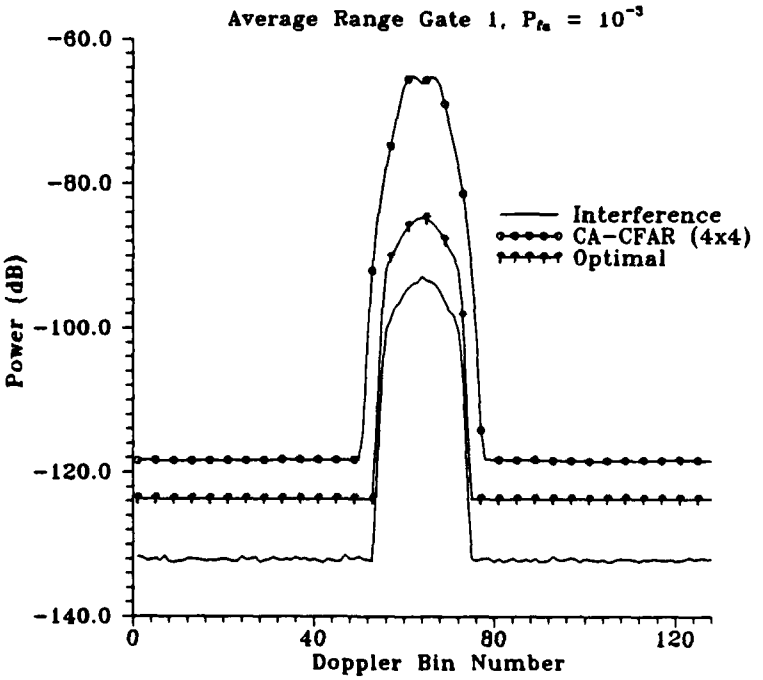

Figure 15 : Threshold Values, RG1, Sidelook, 1 km

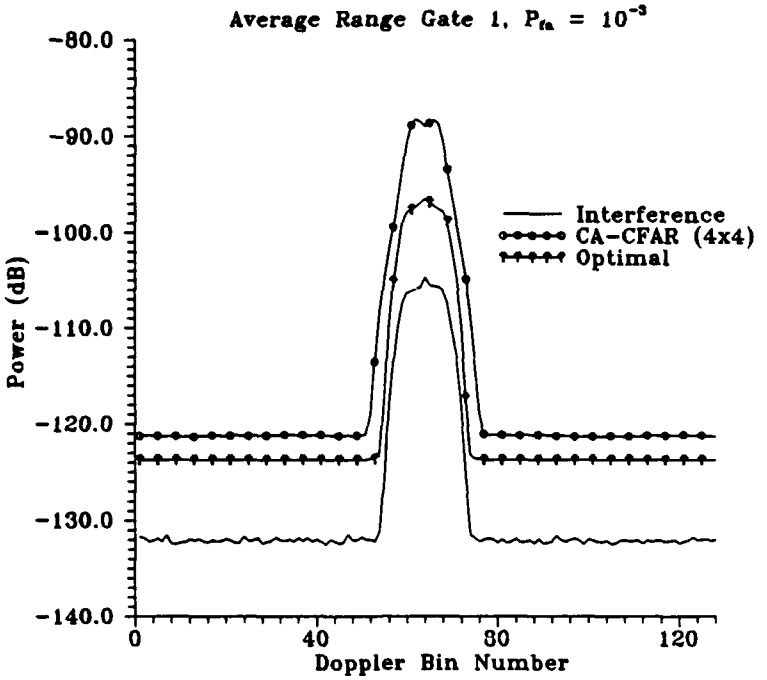

Figure 16 : Threshold Values, RG1, Sidelook, 10 km

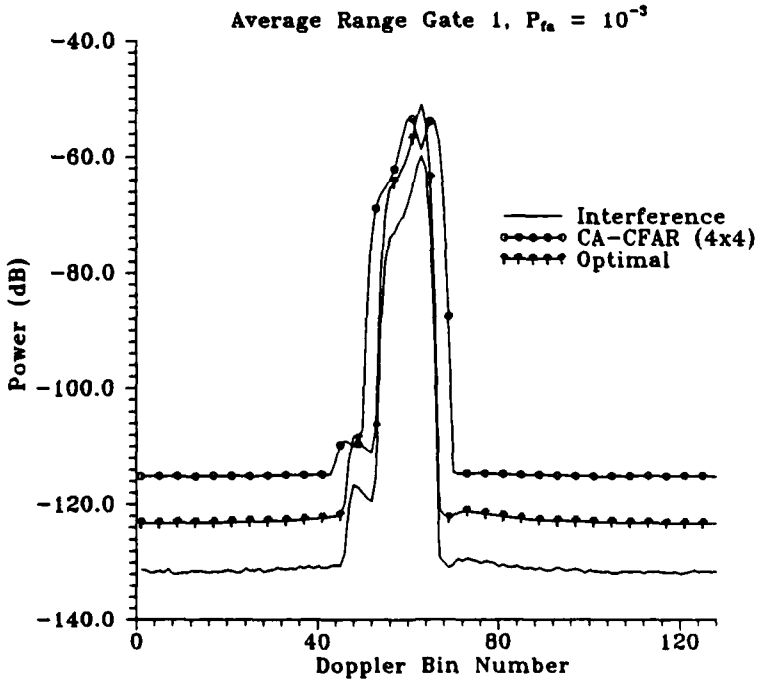

Figure 17 : Threshold Values, RG1, Forward, 100 m

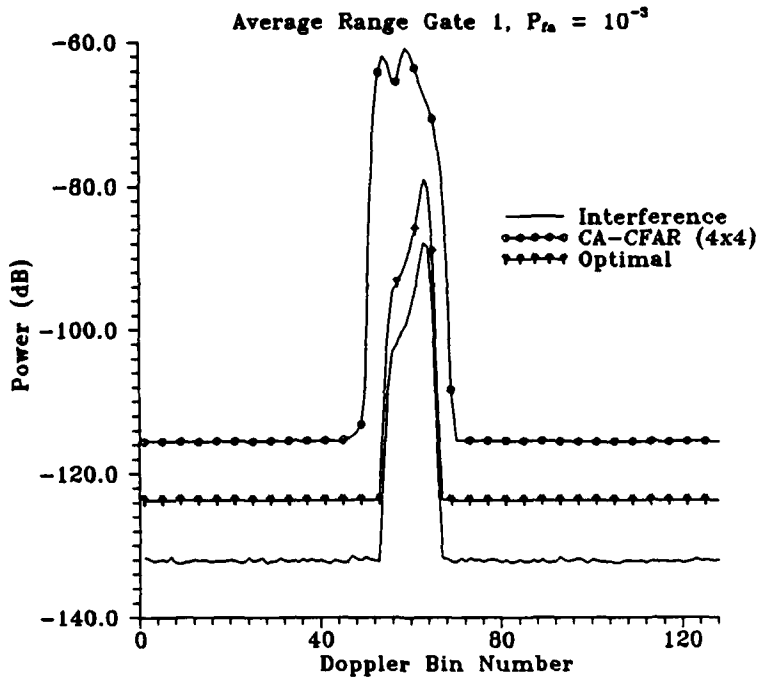

Figure 18 : Threshold Values, RG1, Forward, 1 km

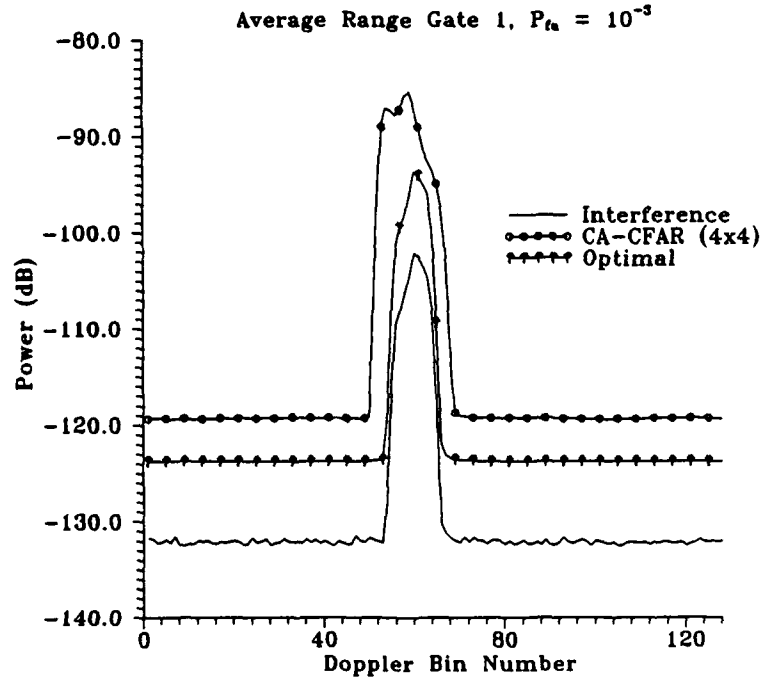

Figure 19 : Threshold Values, RG1, Forward, 10 km

RADAR GEOMETRY	CFAR LOSS IN DECIBELS	
	$P_D = 0.5$	$P_D = 0.9$
Sidelook, Altitude = 100 m	6.2	16.0
Sidelook, Altitude = 1 km	5.5	11.4
Sidelook, Altitude = 10 km	2.7	4.4
Forward, Altitude = 100 m	8.9	37.0
Forward, Altitude = 1 km	8.4	39.0
Forward, Altitude = 10 km	4.5	27.0

TABLE 2 : CA-CFAR (4x4) CFAR Losses

From the threshold plots and Table 2, one can see the effect of the large clutter peak on the performance of the CFAR processor. As the peak decreases in magnitude (increasing altitude), the performance of the processor improves. However, even at an altitude of 10 km, the CFAR processor suffers large CFAR losses when the antenna is pointing in the forward direction. The mean power of cells, on the peak's edge, is likely to be underestimated by the CFAR processor because the reference cell set, for these edge cells, is made up of low powered cells, from the noise dominated interference region. Since underestimation of the cell mean powers contributes most to the CFAR loss [2], it is natural for the performance to degrade in the presence of a large clutter peak.

As will be illustrated in the next section, another effect of the clutter peak is a desensitization of the radar system in the noise dominated interference region. This occurs as a result of the large threshold multiplier, which is required to maintain the false alarm rate in the clutter peak region. This large multiplier causes the threshold in the noise region to be much greater than it need be, resulting in target desensitization. Virtually all of the false alarms which occurred in the simulation (Table 1) took place in the clutter dominated region. Thus, the performance of the processor clearly would improve, if the clutter peak could be negated. A method of achieving this goal is described in the next section.

4.2 Doppler Bin Blanking Cell-Averaging (DBCA-) CFAR

In the previous section, the detrimental effects of the large clutter peak which extends from an approximate Doppler velocity of 500 m/s to -500 m/s, across all five range gates, were examined. As a result, it is suggested that detection of targets in the clutter dominated region not be attempted. In fact, the bins which contain the clutter should not even be included in the

reference cell set for cells in the noise dominated region. In this way, the target detection problem is essentially reduced to the detection of a target in the presence of thermal noise. Increased sensitivity in the noise dominated region would be gained, at the expense of a loss of target detection capability in the clutter peak. However, due to the large power of the clutter in this peak, it is doubtful as to whether a target could possibly be detected in this clutter background in any case. Hence, little system performance would be lost by ignoring the cells which reside in the clutter peak.

It is necessary to develop an adaptive method to locate the bounds of the clutter peak, so as to identify the region which needs to be removed, or blanked, from each individual range-Doppler snapshot. Since the clutter peak is present in all of the range gates, a search in the Doppler dimension, along each range line, can be used to determine which Doppler bins need to be removed. By searching along each individual range gate, complete generalization and flexibility can be achieved by the blanking scheme.

The adaptive blanking algorithm, developed for this work, involves two basic steps, which are performed on each range gate of every snapshot: estimating the interference noise level, and determining the clutter peak region. The first step is accomplished by averaging the interference power in the first and last 30 Doppler bins. These 60 bins were selected because they are well beyond the region in which the clutter peak may be found ($\pm\ v_{ac}$). In order to reduce the effects caused by targets in these Doppler bins, the set of 60 bins may be subdivided into much smaller subsets of two or three bins for averaging. The resulting means from the subsets can then be averaged to obtain an estimate of the background noise floor. Should any subset have a significantly larger mean power than the rest, then it should be excluded from the overall average because it likely contains a target, not just noise.

Once the interference noise power has been approximated, the width of the clutter peak can be estimated. A search is performed, from the positive frequency noise-dominated region (eg. Doppler bin 30) to the centre of the Doppler spectrum (bin 64), for the rising edge of the clutter peak, and from the negative frequency noise-dominated region (eg. bin 90) to the spectrum centre, for the falling edge. The beginning (or end) of the peak is considered to be the first Doppler bin which fulfils a particular "peak location" condition. This condition is satisfied when three consecutive Doppler bins possess interference powers which are greater than three decibels above the estimated noise floor. Note that the "peak location" condition may be made more or less stringent, by varying the required number of consecutive Doppler bins which must exceed the noise floor, or by changing the number of decibels, by which the interference in the Doppler bins must exceed the estimated noise level.

This adaptive Doppler bin blanking algorithm was implemented in conjunction with a 4x4 reference window cell-averaging CFAR processor. In Table 3, the threshold multipliers, which were computed for each of the six radar geometry configurations, are listed. Note that the false alarm rate obtained with the simulated data is close to the desired false alarm rate of 10^{-3}.

RADAR GEOMETRY	C (dB)	ACTUAL P_{FA}
Sidelook, Altitude = 100 m	9.2972	9.2027×10^{-4}
Sidelook, Altitude = 1 km	9.1090	1.0161×10^{-3}
Sidelook, Altitude = 10 km	9.2631	1.0061×10^{-3}
Forward, Altitude = 100 m	9.4017	9.7213×10^{-4}
Forward, Altitude = 1 km	9.1881	9.6039×10^{-4}
Forward, Altitude = 10 km	9.1097	1.0327×10^{-3}

TABLE 3 : Doppler Blanking CA-CFAR (4x4) Threshold Multipliers

By adaptively removing the clutter peak, the interference in all of the range-Doppler maps is reduced to that caused by noise only. Consequently, one would expect to see similar threshold multipliers regardless of the radar geometry and configuration. From the above table, we see that indeed the variation in the threshold multiplier, for the six different cases, has been reduced to 0.293 dB. This means that a single value of the threshold constant can be used to maintain some desired false alarm probability, for all of the radar's operating conditions. This results in a simpler CFAR processing system.

Plots of the threshold distribution function of the Doppler-bin-blanking, cell-averaging (DBCA) CFAR, CA-CFAR, and optimal processors, are shown in Figures 20 to 25, for the six geometric cases. Note that the threshold distribution function curves, for the DBCA-CFAR processor, flatten at values which are less than one, implying a system detection probability which never reaches unity. This is because the blanked Doppler bins have a detection probability of zero, which as explained earlier, has no practical consequence, as it is very unlikely that targets can be detected in the strong clutter peak. However, there is a marked increase in the detection probability of the nonblanked Doppler bins. Table 4 lists the CFAR losses of this DBCA-CFAR processor, for detection probabilities of 0.5 and 0.8, in each of the six geometric conditions. These CFAR losses are much smaller than those of the CA-CFAR processor because the clutter peak has been removed.

The threshold values of the first range gate, averaged over the ensemble of snapshots, are given in Figures 26 to 31, for the six cases studied. No DBCA-CFAR thresholds are plotted in the region which is blanked by the processor. We see that the threshold values of the DBCA-CFAR processor are about four to six decibels lower than the values of the CA-CFAR processor, in the noise-dominated interference region. Hence, the system will have much greater sensitivity to targets in this region, if the clutter peak is removed by the adaptive blanking scheme that has been derived in this work.

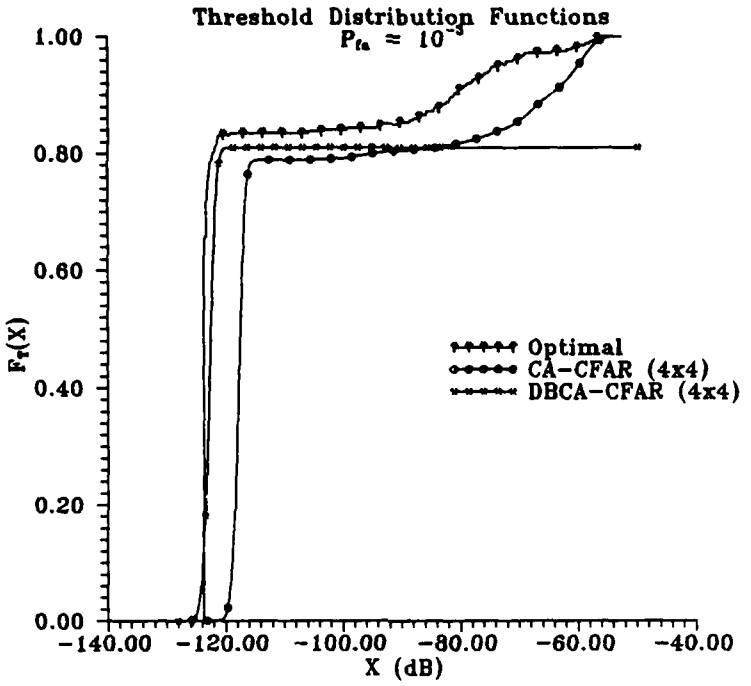

Figure 20: Threshold CDFs - Sidelook, Altitude 100 m

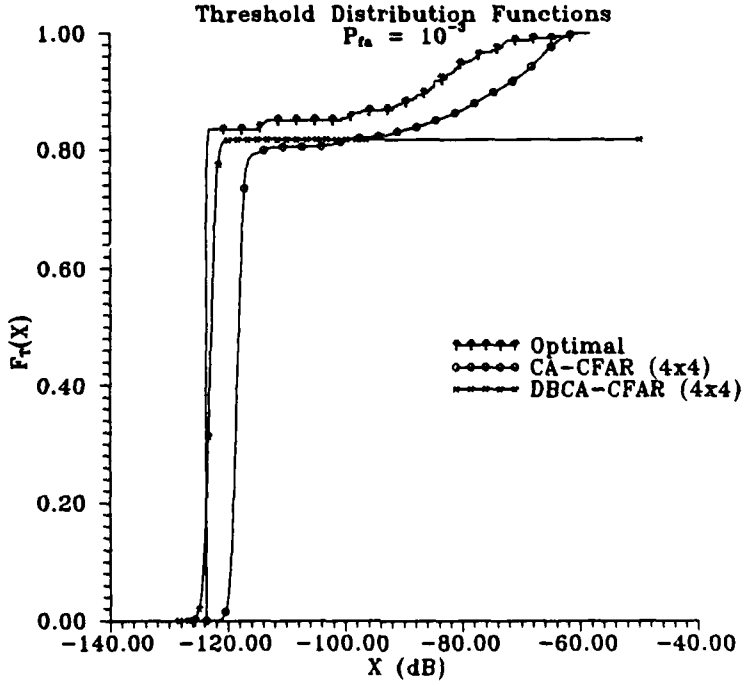

Figure 21: Threshold CDFs - Sidelook, Altitude 1 km

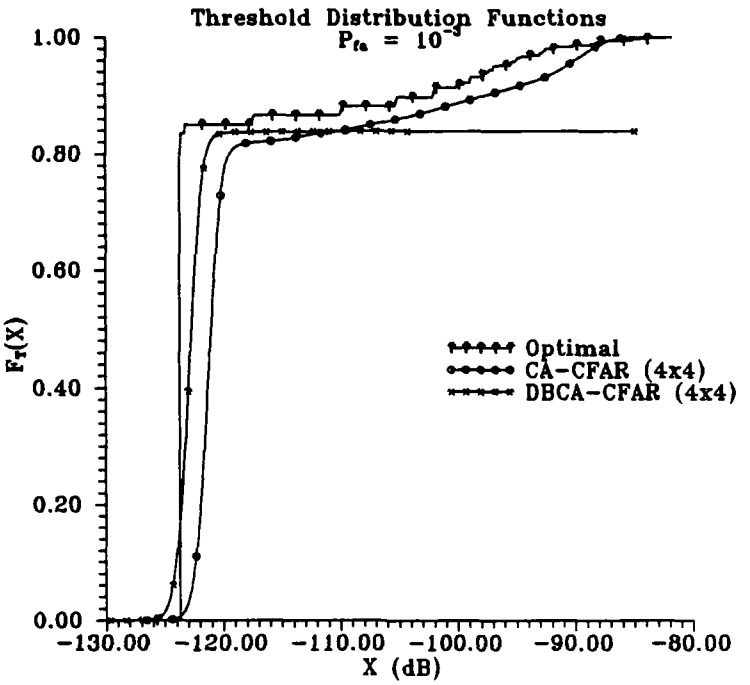

Figure 22: Threshold CDFs - Sidelook, Altitude 10 km

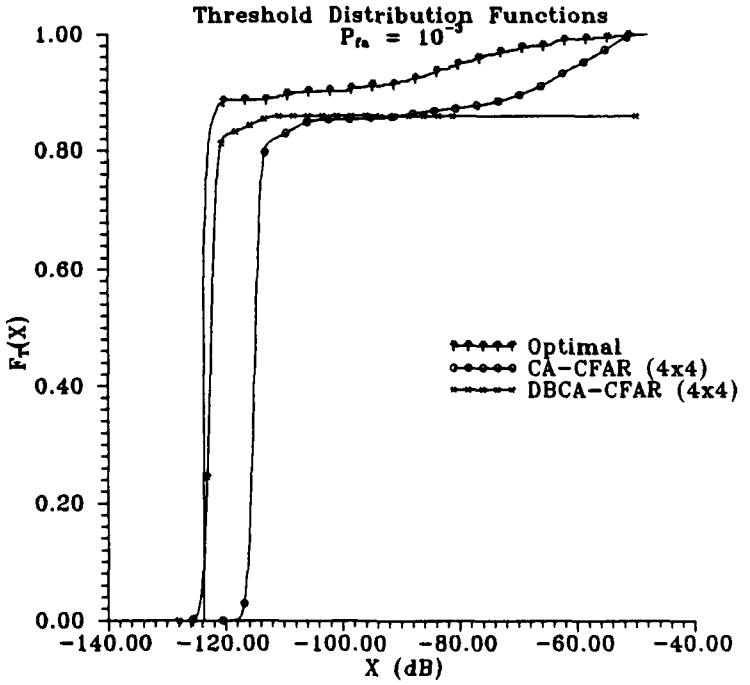

Figure 23: Threshold CDFs - Forward, Altitude 100 m

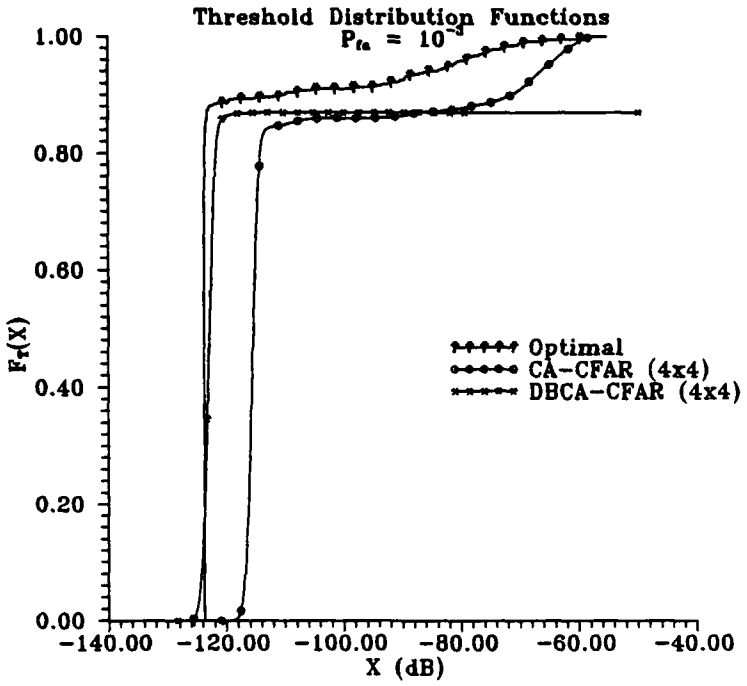

Figure 24: Threshold CDFs - Forward, Altitude 1 km

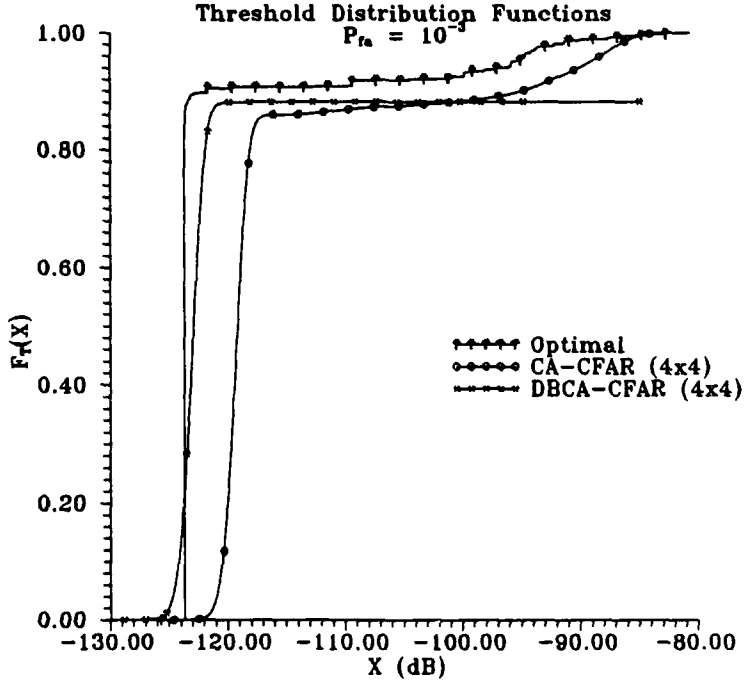

Figure 25: Threshold CDFs - Forward, Altitude 10 km

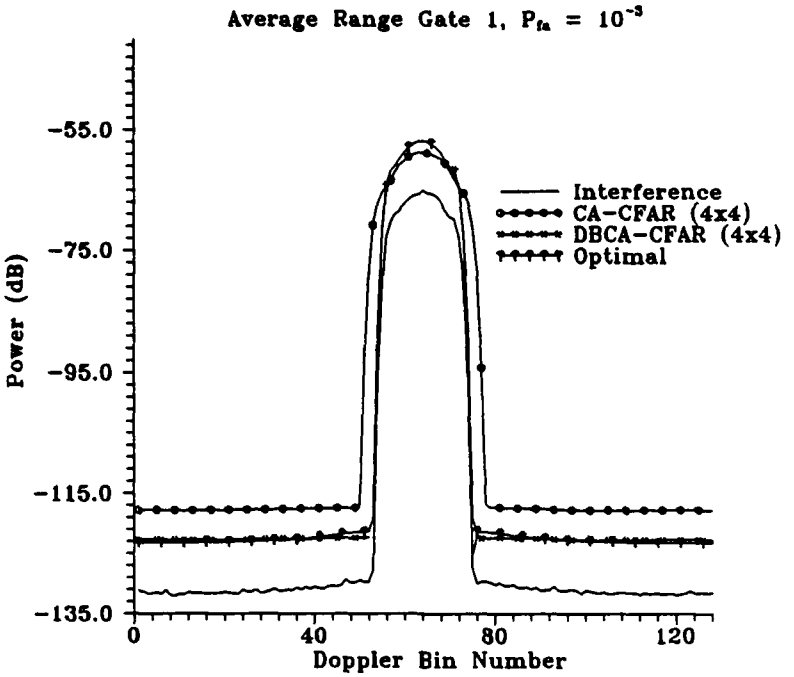

Figure 26 : RG1 Thresholds - Sidelook, Altitude = 100 m

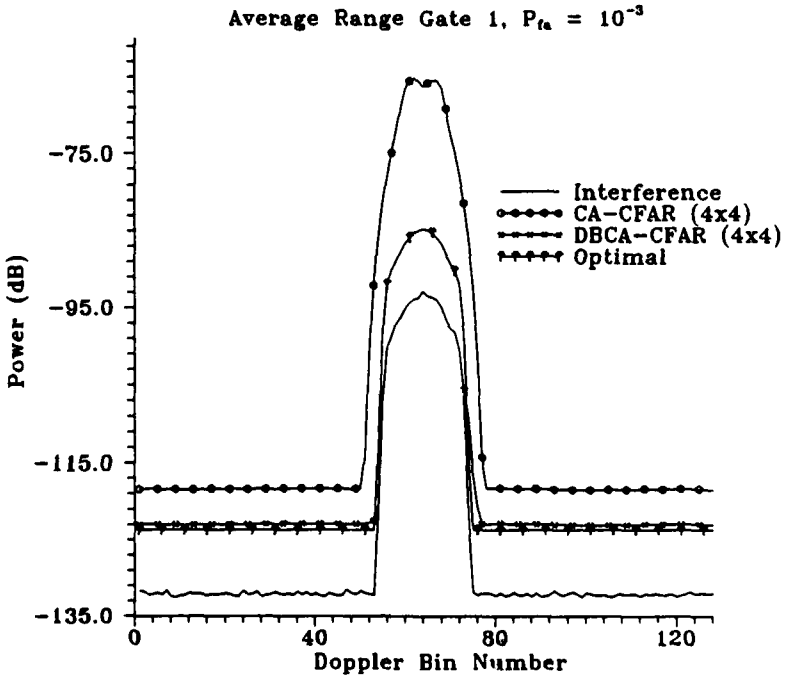

Figure 27 : RG1 Thresholds - Sidelook, Altitude = 1 km

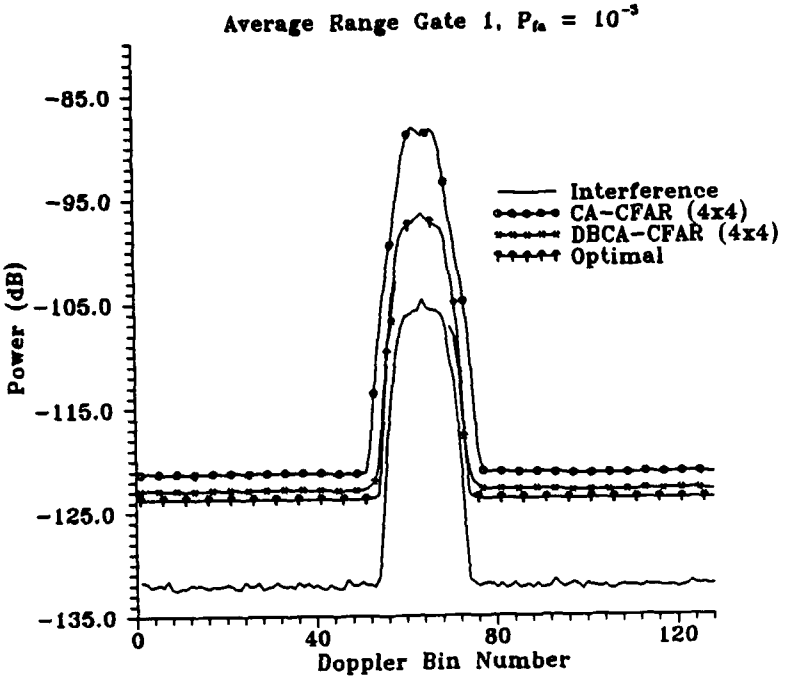

Figure 28 : RG1 Thresholds - Sidelook, Altitude = 10 km

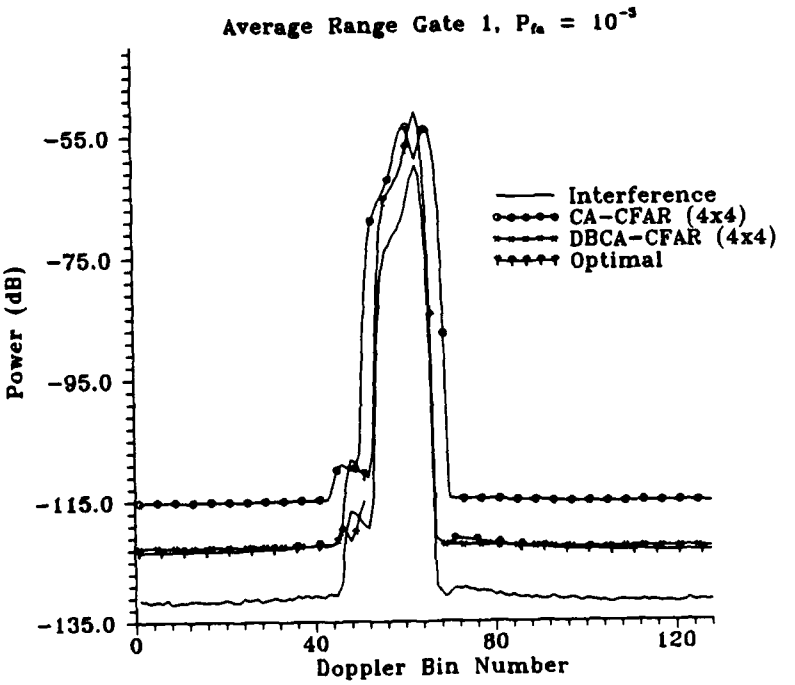

Figure 29 : RG1 Thresholds - Forward, Altitude = 100 m

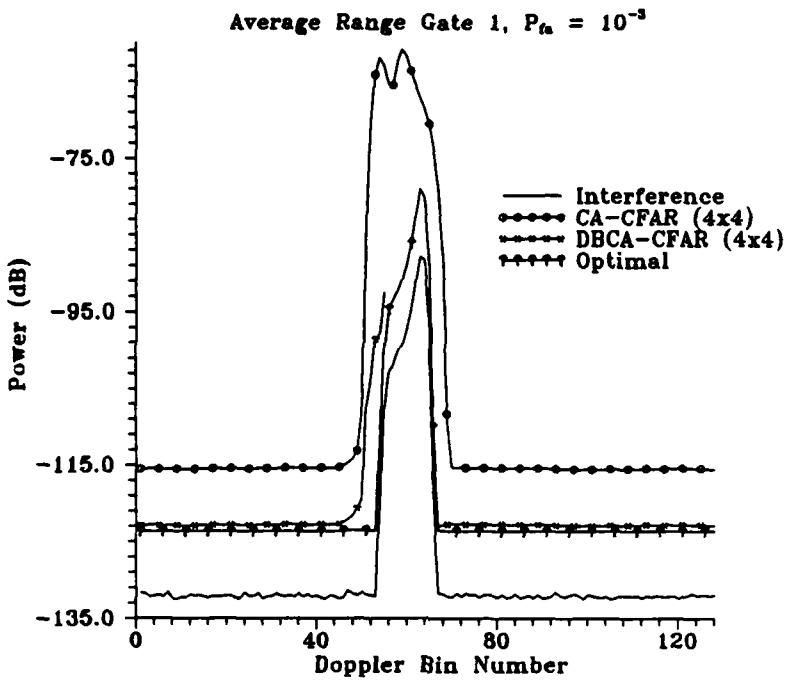

Figure 30 : RG1 Thresholds - Forward, Altitude = 1 km

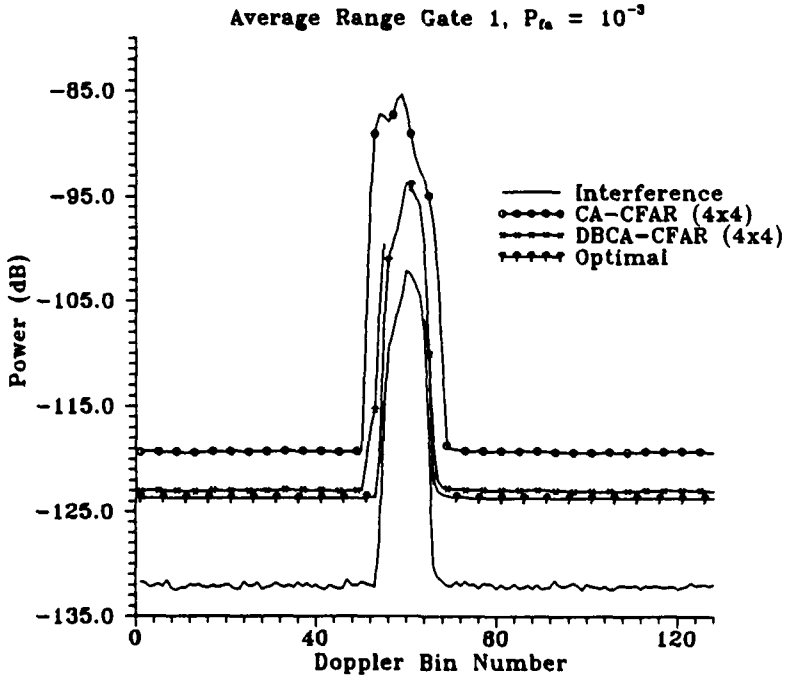

Figure 31 : RG1 Thresholds - Forward, Altitude = 10 km

RADAR GEOMETRY	CFAR LOSS IN DECIBELS	
	$P_D = 0.5$	$P_D = 0.8$
Sidelook, Altitude = 100 m	1.2	1.4
Sidelook, Altitude = 1 km	1.25	1.45
Sidelook, Altitude = 10 km	1.0	2.3
Forward, Altitude = 100 m	1.3	2.0
Forward, Altitude = 1 km	0.9	1.95
Forward, Altitude = 10 km	0.8	1.75

TABLE 4 : DBCA-CFAR (4x4) CFAR Losses

In a previous report [2], it was found that good performance could be achieved through the use of one-dimensional Doppler reference windows. Consequently, the CA-CFAR and DBCA-CFAR processors were also compared using reference windows, which were one-dimensional in the Doppler dimension. In Table 5, the threshold multipliers, computed for the sidelook case at an altitude of 100 m, are listed for each processor. Reference window sizes of 0x10 and 0x40 cells, and a false alarm rate of 10^{-3} have been used in calculating the table. Plots of the threshold distribution functions, and the threshold values for the first range gate, averaged over the ensemble of snapshots, are given in Figures 32 to 35. Once again, from these figures it is evident that the DBCA-CFAR processor outperforms the CA-CFAR processor. Also, as the number of cells in the reference window increases (from 10 to 40), the performance of the DBCA-CFAR processor improves. This is intuitively satisfying, as one would expect an estimate of the mean noise level to improve as the number of samples, used in forming the estimate, increases.

CFAR	REFERENCE SET	C (dB)	ACTUAL P_{FA}
CA-CFAR	0 x 10	10.300	1.0536×10^{-3}
CA-CFAR	0 x 40	13.802	1.0268×10^{-3}
DBCA-CFAR	0 x 10	10.315	1.0084×10^{-3}
DBCA-CFAR	0 x 40	8.980	9.0374×10^{-4}

TABLE 5 : Threshold Multipliers for 0x10, 0x40 Windows

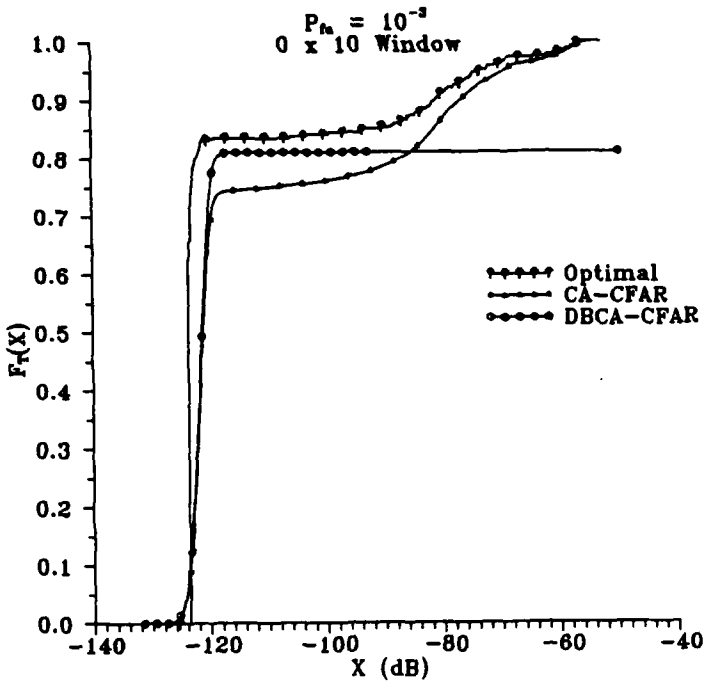

Figure 32 : Threshold CDFs - 0 x 10 Reference Set

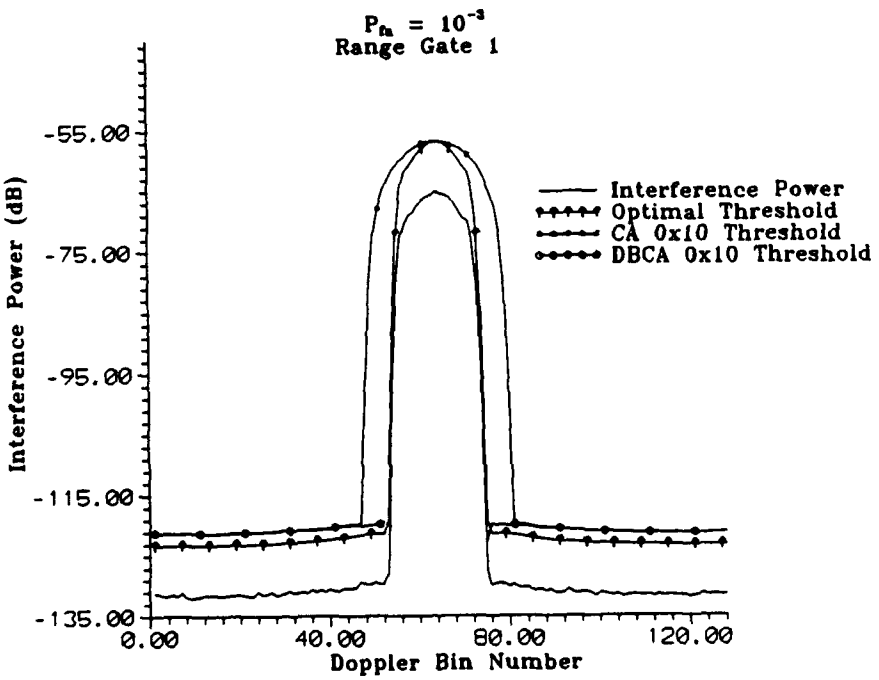

Figure 33 : RG1 Thresholds - 0 x 10 Reference Set

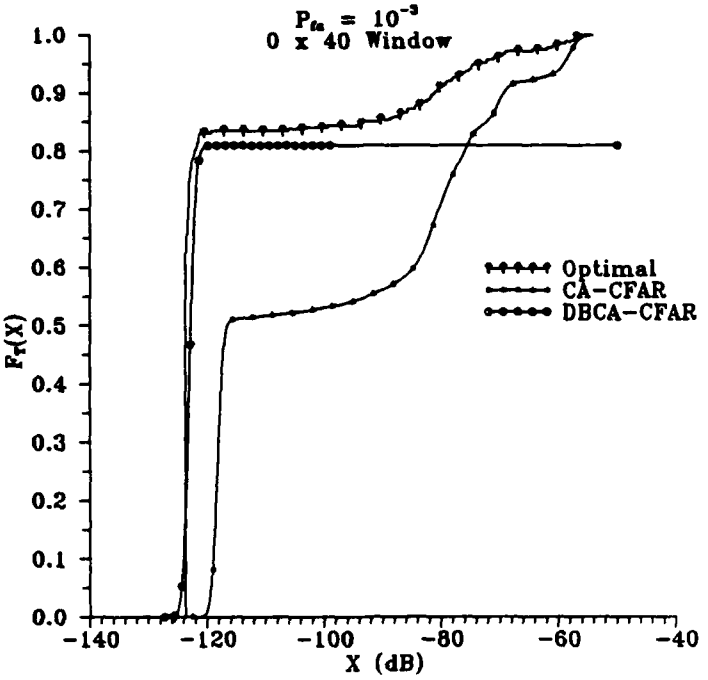

Figure 34 : Threshold CDFs - 0 x 40 Reference Set

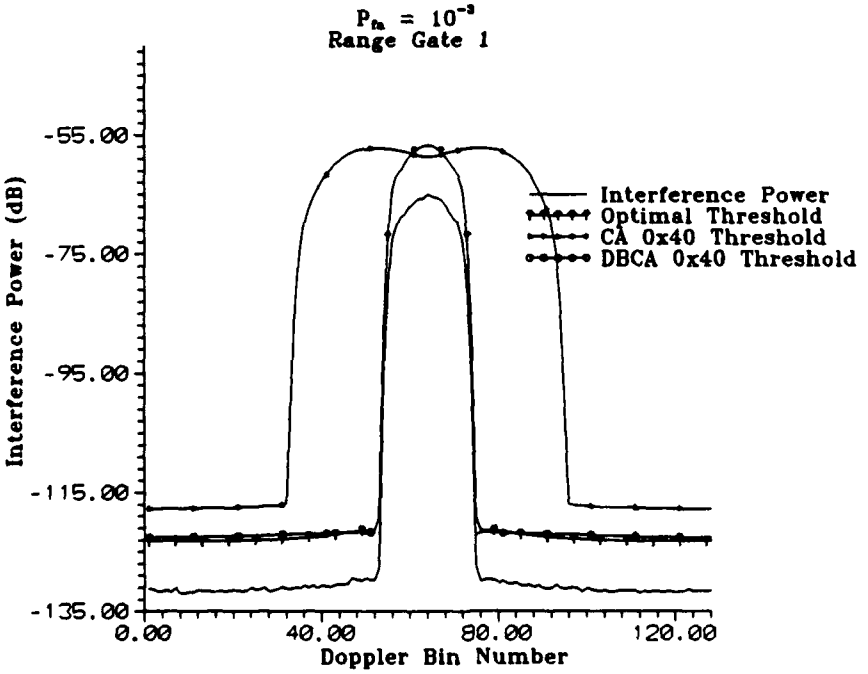

Figure 35 : RG1 Thresholds - 0 x 40 Reference Set

5.0 DETECTION PROBABILITIES

In this section, the detection probabilities of targets of various strengths are obtained through simulation, and compared to theoretical predictions. Non-fluctuating, Swerling Case 0 targets [14] are considered first, followed by Swerling Case 1 fluctuating targets.

To perform detection probability estimates, the CFAR simulator was modified to allow the addition of a steady target to any of the individual range-Doppler cells. A signal, which is composed of a non-fluctuating target plus thermal noise, has a Rician power distribution, as opposed to the exponential power distribution of thermal noise alone [15]. Consequently, an adjustment was made to the simulator to obtain the proper power distribution function, in the cell in which the target resides.

Targets, with various signal-to-noise ratios, were placed in a particular range-Doppler cell, and their detection probabilities were determined by comparing the target cell's power to the threshold computed for that cell. If the cell's power exceeded the threshold, then a detection was declared, otherwise a missed detection was declared. This process was repeated for 10000 snapshots, at which point an estimate of the target's detection probability was obtained. Note that 10000 snapshots yielded estimates which were consistent within approximately one percentage point.

The increased sensitivity to targets, of DBCA-CFAR over CA-CFAR, in the noise-dominated interference region, was demonstrated by calculating the detection probabilities of targets with signal-to-noise ratios of 0,2,4,6,8,10, and 12 dB. The target was placed in Doppler bin 35 of the first range gate for all of the cases. The results are listed in Table 6, along with the theoretical optimal detection probabilities, obtained from Meyer and Mayer [14]. We can see that in general, as expected, the DBCA-CFAR processor yields much larger detection probabilities than the CA-CFAR processor. This is because of the smaller CFAR loss, which is incurred by the DBCA-CFAR processor, and which results in smaller threshold values for any given false alarm rate.

One can confirm the operation of the CFAR simulator, by increasing the target's signal to noise ratio (SNR) by the corresponding processor's CFAR loss. If this is done, then the detection probability should be essentially equivalent to the theoretical value, obtained with an optimal processor, for a target with the original SNR. From the plots of the actual threshold values in the first range gate, it is possible to estimate the additional SNR required to obtain optimal operation, for a target placed in Doppler bin 35. The extra SNR, required for the CA-CFAR processor with reference windows of 4x4, and 0x10 cells, is approximately 5.5 dB, and 2.0 dB, respectively. Note that a 0x40 window, for the CA-CFAR processor, is not considered in this test because of the very large CFAR loss (about 48 dB), associated with this reference window. For the DBCA-CFAR processor, the additional SNRs are 0.5 dB, 2.0 dB, and 0.75 dB, for reference windows of 4x4, 0x10, and 0x40 cells, respectively. Consequently, the detection probability of a CA-CFAR processor using a 4x4 reference window, for a target SNR of 5.5 dB, should be equivalent to an optimal processor detecting a target whose SNR is 0.0 dB.

In Table 7, detection probabilities of an optimal processor, for target SNRs of 0,2,4,6,8,10, and 12 dB, are compared with the CA and DBCA-CFAR processors, whose target SNRs have been increased by the additional SNR mentioned above. From this table, it is clear that by increasing the target's SNR, by an amount equal to the CFAR loss of the processor, the detection rate that would have been obtained using an optimal processor can be achieved. Hence the simulator is working properly.

TARGET SNR (dB)	PERCENTAGE PROBABILITY OF DETECTION						
	OPTIMAL	CA-CFAR			DBCA-CFAR		
		4 x 4	0 x 10	0 x 40	4 x 4	0 x 10	0 x 40
0.0	1.8	0.02	0.75	0.00	2.91	0.75	1.36
2.0	4.0	0.03	1.58	0.00	5.46	1.54	2.79
4.0	9.75	0.07	3.60	0.00	11.74	3.60	6.91
6.0	23.5	0.18	9.18	0.00	24.82	9.18	16.98
8.0	49.0	0.92	23.60	0.00	49.69	23.50	39.11
10.0	81.0	5.34	50.76	0.00	80.02	50.68	71.90
12.0	97.8	24.67	81.61	0.00	96.83	81.60	95.00

TABLE 6 : Detection Probabilities of CA-CFAR and DBCA-CFAR

Finally, some results using Swerling Case 1 targets are presented. Swerling Case 1 targets possess a Rayleigh distributed amplitude, which fluctuates on a scan to scan basis [14]. In Table 8, the detection probabilities, obtained for the CA-CFAR processor, with reference windows of 4x4 and 0x10 cells, and the DBCA-CFAR processor, with reference windows of 4x4, 0x10, and 0x40 cells, are given. Note that the target signal to noise ratios have been increased by the processors' CFAR loss, as with the Case 0 targets, to facilitate a comparison with an optimal processor. Targets with SNRs of 0,2,4,6,8,10, and 12 dB were used. Once again, there is agreement between the theoretical detection probabilities, and the detection probabilities obtained with the CFAR processors, after the CFAR loss has been included in the target's signal to noise ratio.

The small discrepancies between the theoretical detection probabilities, and the simulation results, are believed to be caused by several factors. First, recall that the 10000 snapshots, used to determine the detection rates, produce results which are only consistent to within one percentage point. Inaccurate estimation of the CFAR loss contributes to the error, since even

slight variations of the threshold may cause significant variation in the detection probability. This effect is enhanced for targets with small signal-to-noise ratios. Finally, we note that the detection probabilities obtained are 'local' probabilities. That is, detection was only considered for a target in one particular range-Doppler resolution cell, out of the entire map of cells. A more accurate, 'global', detection probability estimate could be obtained by placing the target in each resolution cell of the map, in turn. This is similar to the manner in which the threshold multiplier was computed. Recall that the estimation errors of every cell, in every snapshot, contribute to the determination of the threshold constant. Analogously, a 'global' detection probability could be obtained. However, this exercise would be extremely time consuming, and somewhat redundant, as a global detection rate can already be computed by using the threshold distribution functions [4]. Hence, little would be gained by conducting a massive simulation to compute 'global' detection probabilities.

OPTIMAL TARGET SNR (dB)	PERCENTAGE PROBABILITY OF DETECTION					
	OPTIMAL	CA-CFAR		DBCA-CFAR		
		4 x 4	0 x 10	4 x 4	0 x 10	0 x 40
0.0	1.8	0.06	1.59	2.95	1.60	1.62
2.0	4.0	0.51	3.82	6.28	3.88	3.63
4.0	9.75	3.18	9.55	13.87	9.50	8.76
6.0	23.5	17.08	23.53	29.34	23.50	23.12
8.0	49.0	55.51	50.15	56.44	50.27	50.99
10.0	81.0	93.57	81.80	85.45	81.81	82.79
12.0	97.8	99.96	97.76	98.56	97.74	98.18

TABLE 7 : Detection Probabilities of CA-CFAR and DBCA-CFAR for Case 0 Targets

OPTIMAL TARGET SNR (dB)	PERCENTAGE PROBABILITY OF DETECTION					
	OPTIMAL	CA-CFAR		DBCA-CFAR		
		4 x 4	0 x 10	4 x 4	0 x 10	0 x 40
0.0	3.1	0.87	0.88	0.85	0.86	0.44
2.0	7.0	4.23	4.04	4.21	4.03	3.31
4.0	14.0	10.72	10.65	10.59	10.67	9.21
6.0	25.0	23.77	21.98	23.48	22.03	20.16
8.0	39.0	37.85	36.03	37.58	36.15	34.96
10.0	54.0	53.58	51.61	53.30	51.64	51.24
12.0	66.5	67.40	65.29	67.17	65.37	65.11

TABLE 8 : Detection Probabilities of CA-CFAR and DBCA-CFAR for Case 1 Targets

6.0 CONCLUSIONS AND RECOMMENDATIONS FOR FURTHER RESEARCH

This report has been an extension of some previous work which was conducted by the authors at DREO [2]. For the particular radar parameters considered, a very large clutter peak (60 dB) extends across all of the range gates, and a segment of the Doppler bins. The returns in the Doppler bins are confined to velocities between the velocity of the radar platform itself, and its corresponding negative value. This clutter peak severely hampers the effectiveness of a CFAR processor, by reducing the sensitivity of the system to targets residing outside of the clutter region. The likelihood of being able to detect any target in this huge clutter return is very small indeed.

Consequently, it was suggested that the range-Doppler cells which contain the clutter be ignored, or 'blanked-out'. In this way, the processor's operating environment is simplified to that required for thermal noise only. A fully adaptive scheme was developed to determine which range-Doppler cells contained the clutter peak, and subsequently, which ones could be ignored in any further processing. By combining this blanking scheme with standard cell-averaging CFAR, substantial reductions in the processor's CFAR loss were achieved. It was shown that the processor which employed the blanking algorithm was much more sensitive to targets in the noise-dominated region of the range-Doppler map.

With the blanking scheme, a single value of the CFAR constant can be used to maintain some desired false alarm rate, in virtually any geometric operating condition of the radar. The

cases which were studied, explicitly included two cases of an airborne radar: one with side-looking, and one with forward-looking antennas. They also included consideration of these two cases at three different altitudes: 100m, 1 km, and 10 km. While the standard CA-CFAR processor's threshold multiplier, exhibited a large variation over these various conditions, the Doppler bin blanking CA-CFAR processor had very little variation. Consequently, there may be no need to recompute the multiplier whenever the geometric parameters change, if the Doppler bin blanking algorithm is used.

Finally, the detection probabilities of non-fluctuating and Swerling Case 1 fluctuating targets were computed, and found to agree with theoretical predictions. This confirmed the proper operation of the CFAR simulator which has been developed.

Future research could investigate the advantages of combining the Doppler bin blanking algorithm, with greatest-of, or ordered statistic CFAR processors [3,16]. In this way, target self masking problems [2,4,12,16] could be reduced, while still benefitting from the performance improvement, obtained through the removal of the clutter peak. Additionally, the Doppler bin blanking algorithm, which has been developed in this report, could be applied to a different set of radar parameters, in which the clutter peak may not be as broad, or strong. This would facilitate testing of the performance of the blanking algorithm, in conjunction with a CFAR processor, in the presence of discrete scatterers, or targets of strength comparable to the clutter returns.

REFERENCES

1. **Finn H.M., and Johnson R.S.,** *Adaptive Detection Mode with Threshold Control as a Function of Spatially Sampled Clutter-Level Estimates,* RCA Review, Vol. 29, No. 3, September 1968, pp. 414-464.

2. **Vrckovnik G., and Faubert D.,** *An Investigation of CFAR Techniques for Airborne Radars,* DREO Report No. 1056, Defence Research Establishment Ottawa, Ottawa, December 1990.

3. **Minkler G., and Minkler J.,** *CFAR : The Principles of Automatic Radar Detection in Clutter,* Magellan Book Company, Baltimore, MD, 1990.

4. **Weber P., Haykin S., and Gray R.,** *Airborne Pulse-Doppler Radar: False-Alarm Control,* IEE Proceedings, Vol. 134, Pt. F, No. 2, April 1987, pp. 127-134.

5. **Press W.H., Flannery B.P., Teukolsky S.A., and Vetterling W.T.,** *Numerical Recipes - The Art of Scientific Computing,* Cambridge University Press, Cambridge, 1986.

6. **Meyer P.L.,** *Introductory Probability and Statistical Applications (Second Edition),* Addison-Wesley Publishing Company, Reading MA, 1970.

7. **Faubert D.,** *A Theoretical Model for Airborne Radars,* Defence Research Establishment Ottawa Report No. 1017, PCN 21LA12, November 1989.

8. **Vineberg K.A., and Saper R.,** *Updates to the DREO Airborne Radar Simulator,* Atlantis Scientific Systems Group Inc. Report No. 167, June 1989.

9. **Gibb M., Lightstone L., and Saper R.,** *Pulse Doppler Radar Simulation Study: Final Technical Report,* Atlantis Scientific Systems Group Inc. Report No. TR-20, October 1988.

10. **Lightstone L.,** *Behaviour of the SIR for Space-Based DPCA Radar Under Various Spatial Clutter Distributions,* Atlantis Scientific Systems Group Inc. Report No. TR-11, February 1988.

11. **Lightstone L.,** *A Model of a Displaced Phase Centre Antenna System for Space-Based Radar with Generalized Orbital Parameters and Earth Rotation,* Atlantis Scientific Systems Group Inc., Contract Number W7714-06-5121, July 1987.

12. **Weiss M.,** *Analysis of Some Modified Cell-Averaging CFAR Processors in Multiple -Target Situations,* IEEE Transactions on Aerospace and Electronic Systems, Vol. AES-18, No. 2, March 1982, pp. 242-248.

13. **Hansen V.G.,** *Constant False Alarm Rate Processing in Search Radars,* IEE Conference Publication No. 105, "Radar-Present and Future", London, October 23-25 1973, pp. 325-332.

14. **Meyer D.P., and Mayer H.A.,** *Radar Target Detection - Handbook of Theory and Practice,* Academic Press, New York, 1973.

15. **Haykin S.,** *Communication Systems, Second Edition,* John Wiley and Sons, New York, 1983.

16. **Rohling H.,** *Radar CFAR Thresholding in Clutter and Multiple Target Situations,* IEEE Transactions on Aerospace and Electronic Systems, Vol. AES-19, No. 4, July 1983, pp. 608-621.

DOCUMENT CONTROL DATA

(Security classification of title, body of abstract and indexing annotation must be entered when the overall document is classified)

1. ORIGINATOR (the name and address of the organization preparing the document. Organizations for whom the document was prepared, e.g. Establishment sponsoring a contractor's report, or tasking agency, are entered in section 8.)

Defence Research Establishment Ottawa
3701 Carling Avenue
Ottawa, Ontario, Canada K1A 0Z4

2. SECURITY CLASSIFICATION (overall security classification of the document including special warning terms if applicable)

UNCLASSIFIED

3. TITLE (the complete document title as indicated on the title page. Its classification should be indicated by the appropriate abbreviation (S,C or U) in parentheses after the title.)

A Doppler Bin Blanking CFAR Processor for Airborne Radars (U)

4. AUTHORS (Last name, first name, middle initial)

VRCKOVNIK Gary E., FAUBERT Denis

5. DATE OF PUBLICATION (month and year of publication of document)	6a. NO. OF PAGES (total containing information. Include Annexes, Appendices, etc.)	6b. NO. OF REFS (total cited in document)
March 1991	42	16

7. DESCRIPTIVE NOTES (the category of the document, e.g. technical report, technical note or memorandum. If appropriate, enter the type of report, e.g. interim, progress, summary, annual or final. Give the inclusive dates when a specific reporting period is covered.)

DREO Technical Report

8. SPONSORING ACTIVITY (the name of the department project office or laboratory sponsoring the research and development. Include the address.)

Defence Research Establishment Ottawa
3701 Carling Avenue
Ottawa, Ontario, Canada K1A 0Z4

9a. PROJECT OR GRANT NO. (if appropriate, the applicable research and development project or grant number under which the document was written. Please specify whether project or grant)	9b. CONTRACT NO. (if appropriate, the applicable number under which the document was written)
021LA	

10a. ORIGINATOR'S DOCUMENT NUMBER (the official document number by which the document is identified by the originating activity. This number must be unique to this document.)	10b. OTHER DOCUMENT NOS. (Any other numbers which may be assigned this document either by the originator or by the sponsor)
DREO Report 1073	

11. DOCUMENT AVAILABILITY (any limitations on further dissemination of the document, other than those imposed by security classification)

(X) Unlimited distribution
( ) Distribution limited to defence departments and defence contractors; further distribution only as approved
( ) Distribution limited to defence departments and Canadian defence contractors; further distribution only as approved
( ) Distribution limited to government departments and agencies; further distribution only as approved
( ) Distribution limited to defence departments; further distribution only as approved
( ) Other (please specify):

12. DOCUMENT ANNOUNCEMENT (any limitation to the bibliographic announcement of this document. This will normally correspond to the Document Availabilty (11). However, where further distribution (beyond the audience specified in 11) is possible, a wider announcement audience may be selected.)

UNCLASSIFIED

SECURITY CLASSIFICATION OF FORM

13. ABSTRACT (a brief and factual summary of the document. It may also appear elsewhere in the body of the document itself. It is highly desirable that the abstract of classified documents be unclassified. Each paragraph of the abstract shall begin with an indication of the security classification of the information in the paragraph (unless the document itself is unclassified) represented as (S), (C), or (U). It is not necessary to include here abstracts in both offical languages unless the text is bilingual).

In this report a novel scheme for adaptively "blanking-out" the radar resolution cells which contain high clutter interference is developed and investigated. For the particular set of radar parameters that are used, a 60 dB clutter peak appears across all of the range gates, and many of the Doppler bins. If not dealt with, this huge peak severely degrades the performance of the CFAR processor, and reduces the sensitivity of the system to targets which reside outside of the clutter region. Our technique consists of adaptively excluding from the decision process the range-Doppler cells located within this clutter peak region. As a result, the performance in the noise dominated interference region is greatly enhanced. Blanking out the clutter peak also reduces the variation which occurs in the values of the CFAR threshold multiplier over various geometric conditions in which the radar may be operated. It is shown that a single value of the CFAR constant can maintain the false alarm rate for large differences in the operating environment of the radar, if Doppler bin blanking is employed. Consequently, a much simpler CFAR processor can be implemented.

14. KEYWORDS, DESCRIPTORS or IDENTIFIERS (technically meaningful terms or short phrases that characterize a document and could be helpful is cataloguing the document. They should be selected so that no security classification is required. Identifiers, such as equipment model designation, trade name, military project code name, geographic location may also be included. If possible keywords should be selected from a published thesaurus, e.g. Thesaurus of Engineering and Scientific Terms (TEST) and that thesaurus-identified. If it is not possible to select indexing terms which are Unclassified, the classification of each should be indicated as with the title.)

Constant false alarm rate processors, CFAR, Cell-averaging, Airborne pulse-Doppler radar, clutter cancellation

UNCLASSIFIED

SECURITY CLASSIFICATION OF FORM